Numerical Analysis of the Rotational Magnetic Springs for EDS Maglev Train

Gang Lv, *Fellow, IET*, Yaqing Liu, Zhixuan Zhang, and Xiaodong Li

***Abstract*—Different from the traditional railway trains, the combined levitation and guidance EDS maglev train is more likely to rotate after being disturbed. Therefore, the rotational electromagnetic stiffnesses are significant operating parameters for the train. In this paper, the different effects of each translational offset generated in the rotational motion on the corresponding rotational electromagnetic stiffnesses in the EDS maglev train are analyzed and calculated. Firstly, a three-dimensional model of the maglev train is established. Then, based on the space harmonic method and the equivalent circuit of the levitation and guidance circuits, the formulas of rolling, pitching and yawing stiffness are presented. Finally, by comparing with the three-dimensional finite element simulation results, the key translational displacements in the rotational motion which has a great impact on the stiffness are obtained. Hence, the three-dimensional analytical formula can be simplified and the computation can be reduced. In addition, the accuracy of the calculation results is verified by comparing with the experimental data of Yamanashi test line.**

***Index Terms*—Magnetic spring, EDS maglev train, electrodynamic, rotational motion, rolling stiffness, pitching stiffness, yawing stiffness**

I. Introduction

As high-speed transportation system, Electrodynamic suspension (EDS) maglev train can run at a speed of 500km/h or even higher, which can fill the gap in the transport market between traditional railway vehicles and air transportation, and is expected to become the next generation of high-speed passenger transportation tools [1]-[2]. The structure of EDS maglev train is described in Fig.1. Different from the traditional railway trains [3]-[7] that rely on mechanical interactions between wheels and rails, the unique coils arrangement and the track structure of EDS maglev train determine its large possibility of multi attitude motion, and put forward higher requirements for its electromagnetic dynamic characteristics. The rotational electromagnetic stiffnesses will not only determine the operation stability of EDS maglev train, but also have a partial impact on the lifting speed of the train [2], thus affecting the actual maintenance cost of the landing gear and guide wheel used by the train at low speed. Therefore, it is particularly necessary to investigate the rotational electromagnetic stiffness of EDS maglev train.

At present, most scholars have studied the influence of translational motion of combined levitation and guidance EDS maglev train on its electromagnetic characteristics. However, only a few scholars have studied the rotating electromagnetic stiffness of combined levitation and guidance EDS maglev train. In [8], Shunsuke Fujiwara changes the two-dimensional distribution model of vehicle coils by changing the coordinate system, so as to calculate the rotational stiffness, but the calculation amount is large. In [9], Toshiaki Murai et al. used the optimization program to analyze the effect of rolling stiffness on lifting speed. In [10], Takenori Yonezu et al. used computer simulation method to analyze the influence of air gap and magnetomotive force of vehicle coil on rolling stiffness. In [11], Hiroshi Yoshioka et al. introduced the change trend of electromagnetic stiffness, including rotational stiffness, in the actual operation. In [12], Oshiaki Murai established a three-dimensional electromagnetic analytical model of EDS maglev and studied its electromagnetic stiffness. However, the analytical model does not analyze the influence of each translational offset on the electromagnetic stiffness when the maglev train rotates.

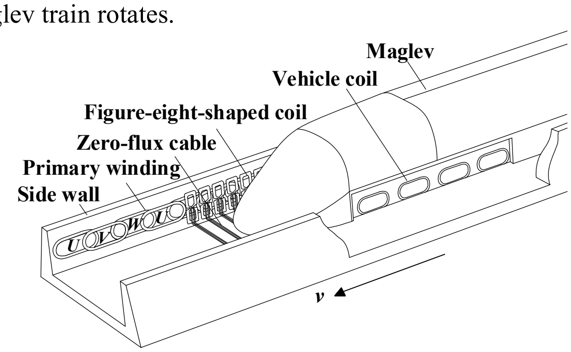

Fig. 1. Structure diagram of EDS maglev train.

In this paper, based on the space harmonic method, by analyzing the influence of translational offset caused by rotational motion on the rotational electromagnetic stiffness of the combined levitation and guidance EDS maglev train, a three-dimensional electromagnetic analytical model and analytical method which can effectively calculate the rotational electromagnetic stiffness of EDS maglev are obtained. The effectiveness of the method is verified by comparing the three-dimensional finite element method (3-D FEM) simulation results with the experimental data of the Yamanashi test line.

Manuscript received January 29, 2022; revised February 18, 2022; accepted March 3, 2022. date of publication March 25, 2022; date of current version March 18, 2022.

This work was supported in part by the National Natural Science Foundation of China under Grant (52077003 and 51777009). *(Corresponding author: Gang Lv.)*

G. Lv is with the Sch. of E.E., Beijing Jiaotong Univ., Beijing 100044, China (e-mail: ganglv@bjtu.edu.cn)

L. Ya and Z. Zhi are with the Sch. of E.E., Beijing Jiaotong Univ., Beijing 100044, China (e-mail: 20117002@bjtu.edu.cn, 19117037@bjtu.edu.cn)

Xiaodong Li is with the Macau University of Science and Technology,Faculty of Innovation Engineering, Macau, 999078, China. (e-mail: xdli @must.edu.mo)

Digital Object Identifier 10.30941/CESTEMS.2022.00009

II. Derivation of Analytical Method

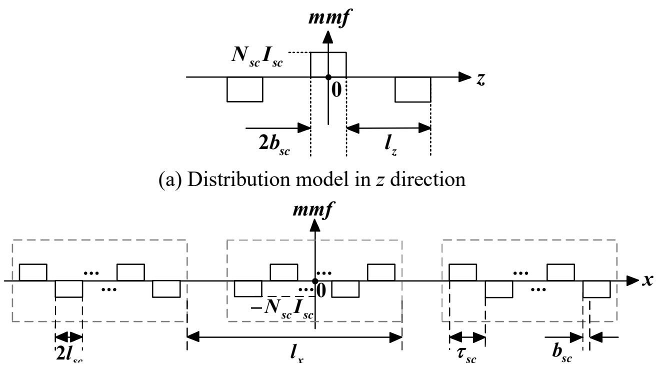

(a) Distribution model in z direction

(b) Distribution model in x direction

Fig. 2. The three-dimensional M.M.F distribution model.

It is assumed that the vehicle coils are a periodically distributed in the x-axis and z-axis and the periods are $2l_x$ and $2l_z$ respectively. The number of the vehicle coils is $2N_2$ on each bogie, the length of it is $2l_{sc}$, the width is $2b_{sc}$, the pitch of it is τ_g, and the M.M.F is $N_{sc}I_{sc}$. According to the three-dimensional magnetomotive force space (3-D M.M.F) model as shown in Fig. 2, the value of y-direction magnetic flux density B_y of vehicle coil where y>0 can be obtained as

$$\dot{B}_y(x,y,z) = C_2 \sum_{n=1}^{\infty}\sum_{m=1}^{\infty} \begin{array}{c} a_m a_n k_l e^{-k_l y}\dot{e}_y \times \\ \cos\left[k_n x + \left(\dfrac{N_2-1}{2}\right)\pi\right]\cos k_m z \end{array} \tag{1}$$

where

$$C_2=\frac{8\mu_0 N_{sc} I_{sc}}{\pi^2},\ a_n=\frac{\sin k_{n1} l_{sc}}{n},\ a_m=\frac{\sin k_m b_{sc}}{m},\ k_m=\frac{m\pi}{l_z},$$

$$k_n=\frac{n\pi}{l_x},\ k_{lj_1}=\sqrt{k_{nj_1}^{\ 2}+k_m^{\ 2}},\ n=1,3,5\cdots\quad m=1,3,5\cdots$$

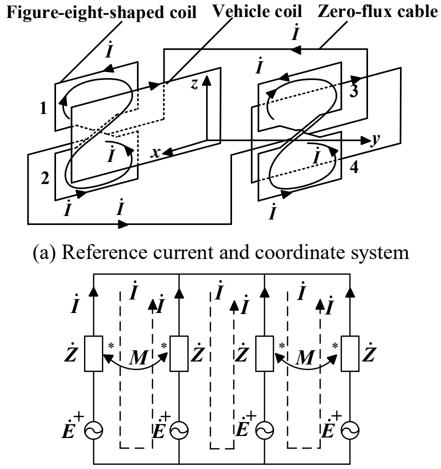

(a) Reference current and coordinate system

(b) Equivalent circuit

Fig. 3. Reference current and equivalent circuit diagram.

As shown in Fig.3(a), the figure-eight-shaped coil is composed of upper unit coil and lower unit coil. And the origin of coordinate system is fixed at the center of bogie, x-axis is always parallel to ground coil, y-axis coincides with zero-flux position line, and z-axis coincides with centering position line. The width of bogie is defined as $2y_c$. The coordinate of the q-th vehicle coil on the bogie is defined as x_q=-$\tau_{sc}q$+5τ_{sc}/2, and the pitch of the figure-eight-shaped coil is τ_g. For the ground figure-eight-shaped coil, its length is $2l_g$, the width is $2b_g$, the number of turns is N_g, the distance between the upper unit coil and lower unit coils is z_g, and the air gap between the figure-eight-shaped coils and the vehicle coils is y_0. When the train is in stable levitation state, the levitation height of the train is h, and the distance between the center of the vehicle coil and the zero-flux position line is z_d. The direction of reference currents and equivalent circuit are shown in Fig. 3(b), since the size and specification of the opposite figure-eight-shaped coil are the same, so $Z_1 = Z_2 = Z_3 = Z_4 = Z$.

For the convenience of calculation, assuming that the train is infinitely thin in z-axis, then the rolling, pitching and yawing motions of the combined levitation and guidance EDS maglev train can be simplified. Then the simplified rotational motion diagram of the train as shown in Fig. 4 can be obtained. The rotation angle of the train is assumed to be positive when the Direction of the rotation motion is as shown in Fig. 4. The red bold lines represent the train, and the blue bold line represents the connecting line of the q-th pair of vehicle coils distributed on both sides of the bogie. It is assumed that the translational displacements of the q-th vehicle coil due to rolling motion are Δy_ϕ and Δz_ϕ, the translational displacements caused by pitching motion are Δx_θ and Δz_θ, and the translational displacements caused by yawing motion are Δx_ψ and Δy_ψ.

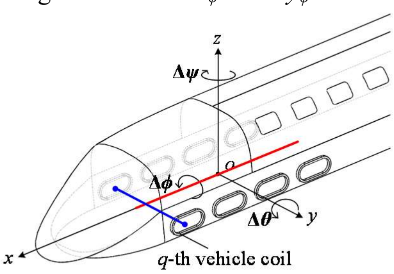

Fig. 4. Schematic diagram of rolling motion, pitching motion and yawing motion of the combined levitation and guidance EDS maglev train.

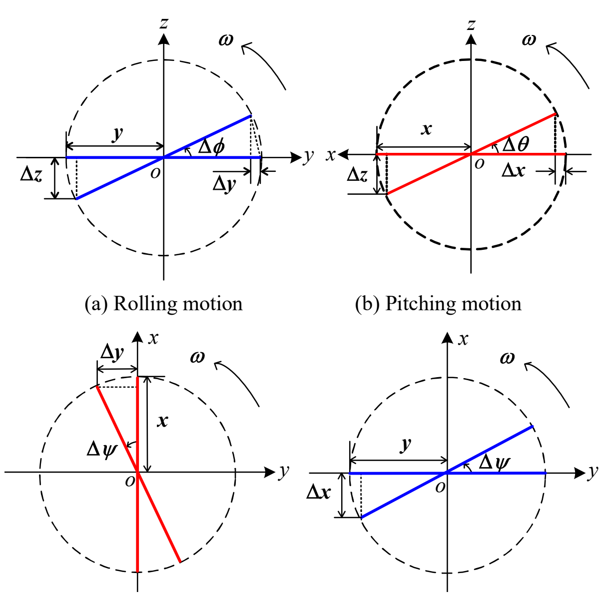

(a) Rolling motion

(b) Pitching motion

(c) Yawing motion

Fig. 5. Simplified rotational motion diagram of maglev train.

Combined with Fig. 4 and Fig. 5, according to the equivalent infinitesimal theorem, since each rotation angle is small, each translational offset can be obtained by

$$\begin{cases}\Delta z_{\phi} = \Delta\phi y_c \\ \Delta y_{\phi}^2 = y_c\left(1-\cos\Delta\phi\right) = 0.5\Delta\phi^2 y_c\end{cases} \tag{2}$$

$$\begin{cases}\Delta z_{\theta} = \Delta\theta x_q \\ \Delta x_{\theta}^2 = y_c\left(1-\cos\Delta\theta\right) = 0.5\Delta\theta^2 x_q\end{cases} \tag{3}$$

$$\begin{cases}\Delta y_{\psi} = \Delta\psi x_q \\ \Delta x_{\psi} = \Delta\psi y_c\end{cases} \tag{4}$$

The flux linkage related to suspension system Ψ_l and the flux linkage related to levitation system Ψ_g can be defined by

$$\Psi_l\left(x,y,z\right) = \sum_{j_1}\left(\Psi_{D_{j_1}} - \Psi_{U_{j_1}}\right) = \sum_{n=1}^{\infty}\sum_{j_1}\Psi_{l_{j_1}} \tag{5}$$

$$\Psi_g\left(x,y,z\right) = \sum_{j_1}\left(\Psi_{D_{j_1}} + \Psi_{U_{j_1}}\right) = \sum_{n=1}^{\infty}\sum_{j_1}\Psi_{g_{j_1}} \tag{6}$$

where

$$\Psi_l = P_l X_1, \Psi_g = P_g X_1, X = e^{j\left[k_n x + \left(\frac{N_2-1}{2}\right)\pi\right]}$$

$$P_l = P_D - P_U = 2\sum_{m=1}^{\infty} C_{P_1} C_l e^{-k_l y_0}, C_l = \sin k_m z_d \sin k_m z_0,$$

$$P_g = P_D + P_U = 2\sum_{m=1}^{\infty} C_{P_1} C_g e^{-k_l y_0}, C_g = \cos k_m z_d \cos k_m z_0,$$

$$C_{P_1} = (-1)^{N_1} 2 n_g C_2 k_l A_1^{sc} A_1^{g},$$

$$A_1^{sc} = \frac{\sin k_n l_{sc} \sin k_m b_{sc}}{mn}, A_{j_1}^{g} = \frac{\sin k_{n_{j_1}} l_g \sin k_m b_g}{mn}$$

The electromotive force (E.M.F) changes of the figure-eight-shaped coil caused by rolling, pitching and yawing motions are defined as $\Delta\Psi_{\phi}$, $\Delta\Psi_{\theta}$ and $\Delta\Psi_{\psi}$ respectively. The variation of E.M.F in upper unit coils and lower unit coils are expressed by subscript U and D respectively. According to Fig.3, the E.M.F of each unit coil $\dot{E}$ can be obtained as follows:

$$\begin{cases}\dot{E}_1 = -j\omega\begin{bmatrix}\Psi_U + \left(\Delta\Psi_{U_{\Delta z_\phi}} + \Delta\Psi_{U_{\Delta y_\phi}}\right) + \\ \left(-\Delta\Psi_{U_{\Delta z_\theta}} - \Delta\Psi_{U_{\Delta x_\theta}}\right) + \left(\Delta\Psi_{U_{\Delta x_\psi}} - \Delta\Psi_{U_{\Delta y_\psi}}\right)\end{bmatrix} \\ \dot{E}_2 = -j\omega\begin{bmatrix}\Psi_D + \left(\Delta\Psi_{D_{\Delta z_\phi}} + \Delta\Psi_{D_{\Delta y_\phi}}\right) + \\ \left(-\Delta\Psi_{D_{\Delta z_\theta}} - \Delta\Psi_{D_{\Delta x_\theta}}\right) + \left(\Delta\Psi_{D_{\Delta x_\psi}} - \Delta\Psi_{D_{\Delta y_\psi}}\right)\end{bmatrix} \\ \dot{E}_3 = -j\omega\begin{bmatrix}\Psi_U - \left(\Delta\Psi_{U_{\Delta z_\phi}} - \Delta\Psi_{U_{\Delta y_\phi}}\right) + \\ \left(-\Delta\Psi_{U_{\Delta z_\theta}} - \Delta\Psi_{U_{\Delta x_\theta}}\right) + \left(-\Delta\Psi_{U_{\Delta x_\psi}} + \Delta\Psi_{U_{\Delta y_\psi}}\right)\end{bmatrix} \\ \dot{E}_4 = -j\omega\begin{bmatrix}\Psi_D - \left(\Delta\Psi_{D_{\Delta z_\phi}} - \Delta\Psi_{D_{\Delta y_\phi}}\right) + \\ \left(-\Delta\Psi_{D_{\Delta z_\theta}} - \Delta\Psi_{D_{\Delta x_\theta}}\right) + \left(-\Delta\Psi_{D_{\Delta x_\psi}} + \Delta\Psi_{D_{\Delta y_\psi}}\right)\end{bmatrix}\end{cases} \tag{7}$$

According to Kirchhoff's law, $\dot{I}_1$, $\dot{I}_2$ and $\dot{I}_3$ can be solved by

$$\begin{cases}\dot{I}_1 = \dfrac{\dot{E}_4 - \dot{E}_3}{2\dot{Z}_l} + \dfrac{\dot{I}_3}{2} = \displaystyle\sum_{n=1}^{\infty}\frac{\dot{g}_l}{2}\begin{bmatrix}\Psi_l - \Delta\Psi_{l_{\Delta z_\phi}} - \Delta\Psi_{l_{\Delta y_\phi}} - \Delta\Psi_{l_{\Delta z_\theta}} \\ -\Delta\Psi_{l_{\Delta x_\theta}} - \Delta\Psi_{l_{\Delta x_\psi}} + \Delta\Psi_{l_{\Delta y_\psi}}\end{bmatrix} + \dfrac{\dot{I}_3}{2} \\ \dot{I}_2 = \dfrac{\dot{E}_2 - \dot{E}_1}{2\dot{Z}_l} + \dfrac{\dot{I}_3}{2} = \displaystyle\sum_{n=1}^{\infty}\frac{\dot{g}_l}{2}\begin{bmatrix}\Psi_l + \Delta\Psi_{l_{\Delta z_\phi}} + \Delta\Psi_{l_{\Delta y_\phi}} - \Delta\Psi_{l_{\Delta z_\theta}} \\ -\Delta\Psi_{l_{\Delta x_\theta}} + \Delta\Psi_{l_{\Delta x_\psi}} - \Delta\Psi_{l_{\Delta y_\psi}}\end{bmatrix} + \dfrac{\dot{I}_3}{2} \\ \dot{I}_3 = \dfrac{\dot{E}_4 + \dot{E}_3 - \dot{E}_2 - \dot{E}_1}{2\dot{Z}_g} = \displaystyle\sum_{n=1}^{\infty}\dot{g}_g\begin{pmatrix}-\Delta\Psi_{g_{\Delta z_\phi}} - \Delta\Psi_{g_{\Delta y_\phi}} \\ -\Delta\Psi_{g_{\Delta x_\psi}} + \Delta\Psi_{g_{\Delta y_\psi}}\end{pmatrix}\end{cases} \tag{8}$$

where

$$\dot{Z}_l = R + j\omega\left(L-M\right), \dot{Z}_g = R + j\omega\left(L+M\right)$$

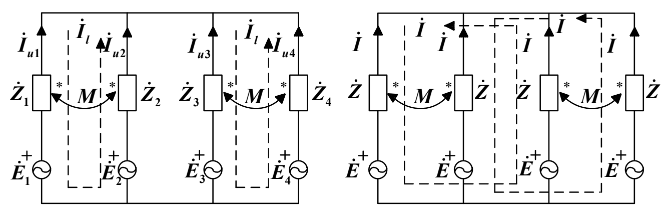

(a) Levitation system (b) Guidance system

Fig. 6. Equivalent circuits.

According to the current relationship shown in Fig. 3 and Fig. 6, it can be obtained that the induced current $\dot{I}_u$ in the unit coil is as follows

$$\begin{cases}\dot{I}_{u1} = -\dot{I}_2 = -\dot{I}_l - \dot{I}_g^U \\ \dot{I}_{u2} = \dot{I}_2 - \dot{I}_3 = \dot{I}_l - \dot{I}_g^D \\ \dot{I}_{u3} = \dot{I}_3 - \dot{I}_1 = -\dot{I}_l + \dot{I}_g^U \\ \dot{I}_{u4} = \dot{I}_1 = \dot{I}_l + \dot{I}_g^D\end{cases} \tag{9}$$

According to the equivalent circuits shown in Fig. 5, the levitation current $\dot{I}_{l_q}$, the guidance current of upper guidance circuit $\dot{I}_{g_q}^U$ and the guidance current of lower guidance circuit $\dot{I}_{g_q}^D$ coupled with the q-th vehicle coil can be obtained by using (7) to (8).

$$\begin{cases}\dot{I}_{l_q} = \dfrac{1}{2}\displaystyle\sum_{n=1}^{\infty}\dot{g}_l\begin{pmatrix}\Psi_l\left(x_q,y_0,z_d\right) - \dfrac{\partial\Psi_l\left(x_q,y_0,z_d\right)}{\partial x}\dfrac{\sqrt{x_q}}{\sqrt{2}}\Delta\theta \\ -\dfrac{\partial\Psi_l\left(x_q,y_0,z_d\right)}{\partial z}x_q\Delta\theta\end{pmatrix} \\ \dot{I}_{g_q}^D = \dot{I}_{g_q}^l + \dot{I}_{g_q}^g \\ = \displaystyle\sum_{n=1}^{\infty}\begin{matrix}\dfrac{\dot{g}_l}{2}\begin{pmatrix}\dfrac{\Psi_l\left(x_q,y_0,z_d\right)}{\partial x}\sqrt{x_q}\Delta\psi + \dfrac{\Psi_l\left(x_q,y_0,z_d\right)}{\partial y}x_q\Delta\psi \\ -\dfrac{\Psi_l\left(x_q,y_0,z_d\right)}{\partial y}\dfrac{\sqrt{y_c}}{\sqrt{2}}\Delta\phi - \dfrac{\Psi_l\left(x_q,y_0,z_d\right)}{\partial z}y_c\Delta\phi\end{pmatrix} + \\ \dfrac{\dot{g}_g}{2}\begin{pmatrix}\dfrac{\Psi_g\left(x_q,y_0,z_d\right)}{\partial x}\sqrt{x_q}\Delta\psi + \dfrac{\Psi_g\left(x_q,y_0,z_d\right)}{\partial y}x_q\Delta\psi \\ -\dfrac{\Psi_l\left(x_q,y_0,z_d\right)}{\partial y}\dfrac{\sqrt{y_c}}{\sqrt{2}}\Delta\phi - \dfrac{\Psi_g\left(x_q,y_0,z_d\right)}{\partial z}y_c\Delta\phi\end{pmatrix}\end{matrix}\end{cases} \tag{10}$$

$$\begin{cases} \dot{I}^{U}_{g_q} = -\dot{I}^{l}_{g_q} + \dot{I}^{g}_{g_q} \\ = \displaystyle\sum_{n=1}^{\infty} \left[\frac{-\dot{g}_l}{2} \left(\begin{aligned} &\frac{\Psi_l\left(x_q, y_0, z_d\right)}{\partial x}\sqrt{x_q}\Delta\psi + \frac{\Psi_l\left(x_q, y_0, z_d\right)}{\partial y} x_q \Delta\psi \\ &-\frac{\Psi_l\left(x_q, y_0, z_d\right)}{\partial y}\frac{\sqrt{y_c}}{\sqrt{2}}\Delta\phi - \frac{\Psi_l\left(x_q, y_0, z_d\right)}{\partial z} y_c \Delta\phi \end{aligned} \right) + \frac{\dot{g}_g}{2} \left(\begin{aligned} &\frac{\Psi_g\left(x_q, y_0, z_d\right)}{\partial x}\sqrt{x_q}\Delta\psi + \frac{\Psi_g\left(x_q, y_0, z_d\right)}{\partial y} x_q \Delta\psi \\ &-\frac{\Psi_l\left(x_q, y_0, z_d\right)}{\partial y}\frac{\sqrt{y_c}}{\sqrt{2}}\Delta\phi - \frac{\Psi_g\left(x_q, y_0, z_d\right)}{\partial z} y_c \Delta\phi \end{aligned} \right) \right] \end{cases} \tag{11}$$

where

$$\dot{g}_l = \frac{j\omega}{\dot{Z}_l}, \dot{g}_g = \frac{j\omega}{\dot{Z}_g}$$

Thus, the rolling stiffness $F_{\phi\phi}$, pitching stiffness $F_{\theta\theta}$ and yawing stiffness $F_{\psi\psi}$ on a bogie can be obtained based on virtual displacement method as follows

$$\begin{aligned} F_{\phi\phi} &= \sum_{q=1}^{N_2} \frac{\partial F_{\phi_q}}{\partial \phi} = \sum_{q=1}^{N_2} \frac{\partial \left(\sum_{p=1}^{4} \dot{I}_{up_q} \frac{\partial \Psi_{up_q}}{\partial \phi} \right)}{\partial \phi} \\ &= \sum_{q=1}^{N_2} y_c^2 F_{ll_q} + \frac{y_c}{2} F_{gg_q} + y_c \sqrt{2 y_c} F_{gl_q} \end{aligned} \tag{12}$$

$$\begin{aligned} F_{\theta\theta} &= \sum_{q=1}^{N_2} \frac{\partial F_{\theta_q}}{\partial \theta} = \sum_{q=1}^{N_2} \frac{\partial \left(\sum_{p=1}^{4} \dot{I}_{up_q} \frac{\partial \Psi_{up_q}}{\partial \theta} \right)}{\partial \theta} \\ &= \sum_{q=1}^{N_2} x_q^2 F_{ll_q} + x_q F_{xx_q} + x_q \sqrt{2\left|x_q\right|} F_{xl_q} \end{aligned} \tag{13}$$

$$\begin{aligned} F_{\psi\psi} &= \sum_{q=1}^{N_2} \frac{\partial F_{\psi_q}}{\partial \psi} = \sum_{q=1}^{N_2} \frac{\partial \left(\sum_{p=1}^{4} \dot{I}_{up_q} \frac{\partial \Psi_{up_q}}{\partial \psi} \right)}{\partial \psi} \\ &= \sum_{q=1}^{N_2} x_q^2 F_{gg_q} + y_c^2 F_{xx_q} + 2 x_q y_c F_{xg_q} \end{aligned} \tag{14}$$

where

$$F_{l_q} = \sum_{p=1}^{4} \dot{I}_{up_q} \frac{\partial \Psi_{up_q}}{\partial z} = \frac{2\tau_{sc}}{\tau_g} \left\{ \sum_{n=1}^{\infty} \left[\dot{I}_{l_q} \frac{\partial \Psi_{l_q}}{\partial z} + \dot{I}^{l}_{g_q} \frac{\partial \Psi_{l_q}}{\partial z} + \dot{I}^{l}_{g_q} \frac{\partial \Psi_{g_q}}{\partial z} \right] \right\}$$

$$F_{ll_q} = \frac{\partial F_{l_q}}{\partial z}, \quad \begin{aligned} F_{g_q} &= \sum_{p=1}^{4} \dot{I}_{up_q} \frac{\partial \Psi_{up_q}}{\partial y} = F_{g_{1q}} + F_{g_{2q}} + F_{g_{3q}} \\ &= \frac{2\tau_{sc}}{\tau_g} \left\{ \sum_{n=1}^{\infty} \left[\dot{I}_{l_q} \frac{\partial \Psi_{l_q}}{\partial y} + \dot{I}^{l}_{g_q} \frac{\partial \Psi_{l_q}}{\partial y} + \dot{I}^{g}_{g_q} \frac{\partial \Psi_{g_q}}{\partial y} \right] \right\} \end{aligned}$$

$$F_{x_q} = \sum_{p=1}^{4} \dot{I}_{up_q} \frac{\partial \Psi_{up_q}}{\partial x} = \frac{2\tau_{sc}}{\tau_g} \left\{ \sum_{n=1}^{\infty} \left[\dot{I}_{l_q} \frac{\partial \Psi_{l_q}}{\partial x} + \dot{I}^{l}_{g_q} \frac{\partial \Psi_{l_q}}{\partial x} + \dot{I}^{g}_{g_q} \frac{\partial \Psi_{g_q}}{\partial x} \right] \right\}$$

$$\frac{1}{\partial \phi} = \frac{y_c}{\partial z} + \frac{\sqrt{y_c}}{\sqrt{2}\partial y}, \frac{1}{\partial \theta} = \frac{x_q}{\partial z} + \frac{\sqrt{x_q}}{\sqrt{2}\partial x}, \frac{1}{\partial \psi} = \frac{x_q}{\partial y} + \frac{y_c}{\partial x}$$

$$F_{gg_q} = \frac{\partial F_{g_1}}{\partial y} + \frac{F_{g_2} + F_{g_3}}{\Delta y}, F_{ij_q} = \frac{\partial F_{i_q}}{\partial j}, i = l, g, x, j = x, y, z,$$

III. Characteristic Calculation And Experimental Validation

According to the basic parameters of levitation and guidance system as shown in Table I, rolling stiffness, pitching stiffness and yawing stiffness are calculated. In order to further analyze and verify the influence of translational offset on the rotational electromagnetic stiffnesses, this paper compares the numerical calculated results with the 3-D FEM simulation results and experimental data.

TABLE I
Basic Parameters of Levitation And Guidance System of MLX01[13]-[15].

Symbol	Value	Quantity
$2l_{sc}$	1.07m	Length of the vehicle coil
$2b_{sc}$	0.5m	Width of the vehicle coil
τ_{sc}	1.35m	Pitch of the vehicle coil
N_{sc}	1400	Turns of the vehicle coil
I_{sc}	500A	Current of single turn vehicle coil
N_2	4	Number of vehicle coils on one side of each bogie
z_d	0.04m	Distance between the center line of the vehicle coil and zero-flux position line when the maglev is in stable suspension
$2l_g$	0.35m	Length of the unit coil
$2b_g$	0.34m	Width of the unit coil
τ_g	0.45m	Pitch of the unit coil
N_g	24	Turns of the unit coil
y_0	0.185m	Transverse distance between vehicle coil and ground figure-eight-shaped coil
R	0.256mH	Resistance of unit coil
L	3.6mH	Inductance of unit coil
M	18.4μH	Mutual inductance of unit coil
z_g	0.08m	Vertical distance between unit coils
$2y_c$	2.98m	Width of the bogie

A. Rolling Motion

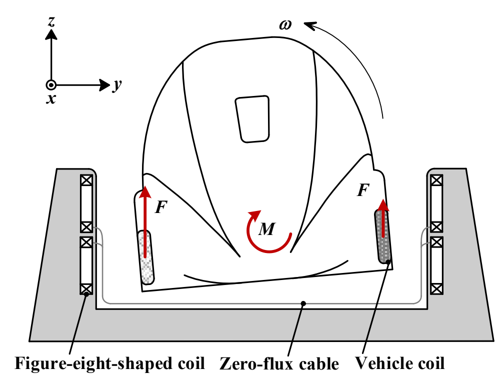

Fig. 7. Rolling torque M_ϕ when the combined levitation and guidance EDS maglev train rolls after being disturbed.

When the combined levitation and guidance EDS maglev train rolls clockwise after being disturbed, as shown in Fig.7, the left vehicle coil sinks and the right vehicle coil rises, resulting in the increase in the coupling area between the left vehicle coil and the lower unit coil and the decrease in the coupling area between the right vehicle coil and the lower unit coil. Therefore, the levitation force on the left vehicle coil increases and the levitation force on the right vehicle coil decreases. Thus, according to Lenz's law, a counterclockwise rolling torque M_ϕ as shown in Fig. 7 is generated, and its direction is just opposite to the direction of rolling motion. In conclusion, the combined levitation and guidance EDS maglev train has the ability to resist rolling disturbance, that is, its rolling stiffness $F_{\phi\phi}$ is positive. In addition, it is obvious that the rolling stiffness $F_{\phi\phi}$ is the key parameter in the design stage of the train.

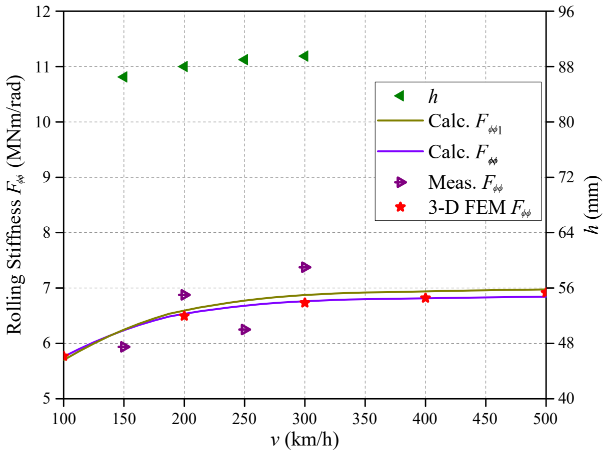

Fig. 8. The trend of $F_{\phi\phi}$ and $F_{\phi\phi 1}$ with v.

Definition $F_{\phi\phi 1}$ is a function considering variable Δz_ϕ, and $F_{\phi\phi}$ is a function considering variable Δz_ϕ and Δy_ϕ. Fig.8 describes the variation trend of $F_{\phi\phi}$ and $F_{\phi\phi 1}$ obtained by numerical analysis and experimental results with the change of running speed v. It can be seen that rolling stiffness increases gradually with the increase of vehicle running speed v. This means that the maglev train has the better ability to resist rolling disturbance at higher speed.

The relative errors of $F_{\phi\phi}$ and $F_{\phi\phi 1}$ with the experimental results are 6.12% and 6.63%, respectively. In addition, the relative errors of $F_{\phi\phi}$ and $F_{\phi\phi 1}$ with the 3-D FEM results are 0.46% and 1.51%, respectively. By comparing the numerical analysis results with the 3-D FEM simulation results and the experimental results in Fig.8, it can be seen that the relative errors of the $F_{\phi\phi}$ and $F_{\phi\phi 1}$ both are relatively small, which means that the analytical $F_{\phi\phi 1}$ can well describe the rolling stiffness of combined levitation and guidance EDS maglev train. That is, the translational offset in y-axis caused by rolling motion Δy_ϕ can be ignored when establishing the analytical model for analyzing rolling stiffness.

B. *Pitching Motion*

When the combined levitation and guidance EDS maglev train is disturbed and pitching clockwise as shown in Fig.9, No. 1 and No. 2 vehicle coils sink and No. 3 and No. 4 vehicle coils rise. Similarly, since the coupling area between No. 1 and No. 2 vehicle coils and the lower unit coil increases, and the coupling area between No. 3 and No. 4 vehicle coils and the lower unit coil decreases, the levitation force on No. 1 and No. 2 vehicle coils increases, while the levitation force on No. 3 and No. 4 vehicle coils decreases. Due to the uneven levitation force of the vehicle coil distributed along the x-axis, the counterclockwise pitching torque M_θ is generated. Moreover, the direction of pitching torque M_θ is opposite to that of the pitching motion, which shows that the pitching stiffness of the combined levitation and guidance EDS maglev train is positive, that is, the train has the ability to resist pitching disturbance. The quench of vehicle coil and track irregularity will lead to pitching motion, so the pitching stiffness $F_{\theta\theta}$ is a key parameter worth studying for the combined levitation and guidance EDS maglev train.

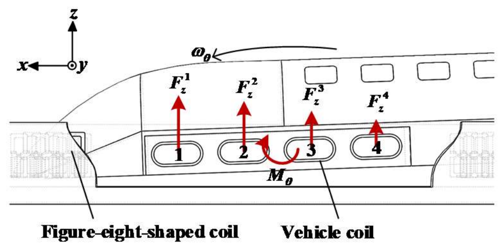

Fig. 9. Pitching torque M_θ when the combined levitation and guidance EDS maglev train pitches after being disturbed.

It is defined that $F_{\theta\theta 1}$ is a function considering variable Δz_θ, and $F_{\theta\theta}$ is a function considering variable Δz_θ and Δx_θ. Fig.10 describes the variation trend of $F_{\theta\theta}$ and $F_{\theta\theta 1}$ obtained by numerical analysis results with the change of running speed v. It can be seen that pitching stiffness increases gradually with the increase of running speed. It can be seen that the values of $F_{\theta\theta}$ and $F_{\theta\theta 1}$ are same, and the relative errors between them and the 3-D FEM results are the same and equal to 2.06%. Therefore, the translation offset in the x-axis Δx_θ caused by pitching motion can be ignored when establishing the model for analyzing pitching stiffness.

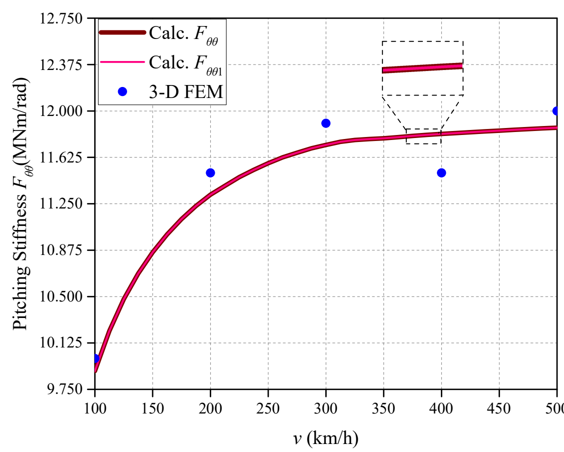

Fig. 10. The trend of $F_{\theta\theta}$ and $F_{\theta\theta 1}$ with running speed v.

C. *Yawing Motion*

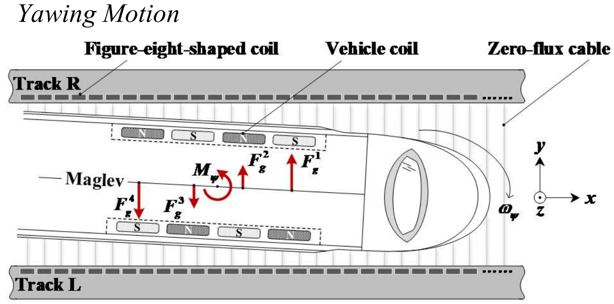

Fig. 11. Pitching torque M_ψ when the combined levitation and guidance EDS maglev train yaws after being disturbed.

When the combined levitation and guidance EDS maglev train is disturbed and yaws counterclockwise as shown in Fig.11, the transverse air-gap of each vehicle coil changes, resulting in unequal induced E.M.F in the ground coils on the positive and negative sides of y-axis coupled with the vehicle coils on the opposite side of the bogie. According to Lenz's law, the guidance force of each pair of vehicle coils is shown in Fig.11. Due to the uneven force in the y-axis, the yawing torque M_ψ in the clockwise direction is generated, and its direction is opposite to the direction of yawing motion. It can be seen that the combined levitation and guidance EDS maglev train has the ability to resist yawing disturbance, and this ability is defined as yawing stiffness.

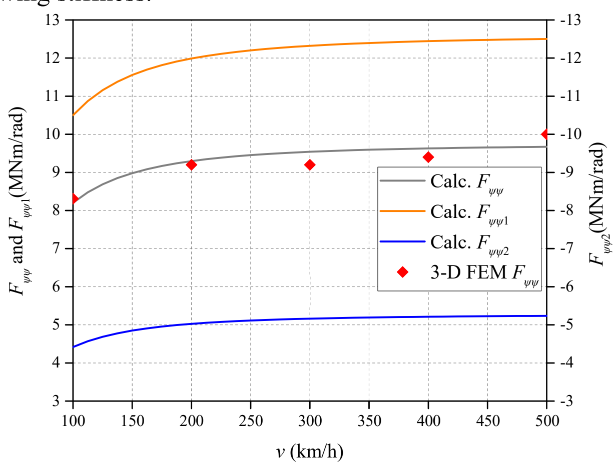

Fig. 12. The trend of $F_{\psi\psi}$, $F_{\psi\psi1}$ and $F_{\psi\psi2}$ with running speed v .

It is defined that $F_{\psi\psi1}$ is a function related to independent variable Δy_ψ, $F_{\psi\psi2}$ is a function related to independent variable Δx_ψ, and $F_{\psi\psi}$ is a function with independent variable Δy_ψ and Δx_ψ. Fig.12 describes the variation trend of $F_{\psi\psi}$ and $F_{\psi\psi1}$ obtained by numerical analysis results with the change of running speed. It can be seen that yawing stiffness increases gradually with the increase of running speed. In addition, as can be seen from Fig. 12, the relative error between $F_{\psi\psi}$ and 3-D FEM results are 2.35%, and the relative error between $F_{\psi\psi1}$ and 3-D FEM results and between $F_{\psi\psi2}$ and 3-D FEM results are 29.60% and 154.35% respectively. Therefore, the translational offsets Δy_ψ and Δx_ψ caused by yawing motion must be considered simultaneously when establishing the model for analyzing yawing stiffness.

IV. Conclusion

In this paper, the effects of translational offsets on the rotational electromagnetic stiffness of EDS maglev are analyzed, and a simplified electromagnetic model of 3-D rotational motion of maglev is proposed. Then the calculation formulas of rolling stiffness, pitching stiffness and yawing stiffness of EDS maglev based on space harmonic method are proposed. And the validity and accuracy of the method are verified by comparing with 3-D FEM results and experimental data of Yamanashi test line. The main conclusions are as follows:

1) The offset in y-axis Δy_ϕ caused by rolling motion can be ignored, and the offset in z-axis Δz_ϕ caused by rolling motion should be considered when establishing the analytical model for analyzing rolling stiffness.
2) The offset in x-axis Δx_θ caused by pitching motion can be ignored, and the offset in z-axis Δz_θ caused by pitching motion should be considered when establishing the analytical model for analyzing pitching stiffness.
3) Both the offset in y-axis Δy_ψ and the offset in x-axis Δx_ψ caused by yawing motion should be considered when establishing the analytical model for analyzing yawing stiffness.
4) With the increase of running speed, the rolling stiffness, pitching stiffness and yawing stiffness increase, which shows that the combined levitation and guidance EDS maglev train has better ability to resist rolling, pitching and yawing disturbances at higher speed.

References

[1] I. Boldea, *Linear Electric Machines, Drives and MAGLEVs Handbook*. CRC Press, 2013.

[2] Hyung-Woo Lee, Ki-Chan Kim and Ju Lee, “Review of maglev train technologies,” *IEEE Transactions on Magnetics*, vol. 42, no. 7, pp. 1917-1925, July 2006

[3] G. Lv, D. Zeng, T. Zhou and Z. Liu, “Investigation of Forces and Secondary Losses in Linear Induction Motor With the Solid and Laminated Back Iron Secondary for Metro,” *IEEE Trans. Ind. Electron.*, vol. 64, no. 6, pp. 4382-4390, June 2017.

[4] G. Lv, T. Zhou, D. Zeng and Z. Liu, “Influence of Secondary Constructions on Transverse Forces of Linear Induction Motors in Curve Rails for Urban Rail Transit,” *IEEE Trans. Ind. Electron.*, vol. 66, no. 6, pp. 4231-4239, June 2019.

[5] G. Lv, S. Yan, D. Zeng and T. Zhou, “An equivalent circuit of the single-sided linear induction motor considering the discontinuous secondary,” *IET Electr. Power Appl.,* vol. 13, no. 1, pp. 31-37, 2019.

[6] Hironori HOSHINO, Erimitsu SUZUKI, Ken WATANABE, “Reduction of Vibrations in Maglev Vehicles Using Active Primary and Secondary Suspension Control,” *Quarterly Report of RTRI*, vol. 49, no. 2, pp. 113-118, June 2008.

[7] Yoshioka, H. and Watanabe, K., “Dynamic Characteristics of Side-wall Magnetically Levitated Vehicle,” *The International Conference on Speedup Technology for Railway and Maglev Vehicles (STECH'93)*, no. PS1-2, pp. 103-108, 1993.

[8] Fujiwara, S., “Characteristics of EDS Magnetic Levitation with Ground Coils for Levitation Arranged on the Side Wall,” *Elect. Eng. Jpn.*, vol. 108, no. 5, pp. 439-446, May. 1988.

[9] Murai, T. and Fujiwara, S., “Design of Coil Specifications in EDS Maglev Using an Optimization Program,” *Proc.of the 2nd International Symposium on Linear Drives for Industry Applications (LDIA'98)*, no. ML-13, pp. 343-346, 1998.

[10] Takenori YONEZU, Ken WATANABE, Erimitsu SUZUKI, Takashi SASAKAWA, “Characteristics of Magnetic Springs for Guidance of Superconducting Maglev Vehicles,” *Quarterly Report of RTRI*, 8 vol. 59, no. 4, pp. 293-298, Nov. 2018.

[11] Yoshioka, H., Suzuki, E., Seino, H., Azakami, M., Oshima, H., and Nakanishi, T., “Characteristics of the Dynamics of the MLX01Yamanashi Maglev Test Line Vehicles,” *Quarterly Report of RTRI*, vol.39, no. 2, pp. 62-67, 1998

[12] Toshiaki Murai, “Characteristics of LSM Combined Propulsion, Levitation and Guidance,” *Elect. Eng. Jpn.*, vol. 114, no. 7-8, pp. 746-752, Jul. 1994.

[13] Fujimoto T, Aiba M, Suzuki H, “Characteristics of electromagnetic force of ground coil for levitation and guidance at the Yamanashi maglev test line,” *Quarterly report of RTRI*, vol. 41, no. 2, pp. 63-67, 2000.

[14] Toshiaki Murai, Takashi Sasakawa, “Characteristics of SC Coil Configuration for EDS Maglev to Reduce Leakage Flux with Strengthened Magnetomotive Force,” *IEEJ Transactions on Industry Applications*, vol. 124, no. 9, pp. 962-967, Dec. 2004

[15] T. Yonezu, H. Hoshino, E. Suzuki and K. Watanabe, "Development of models for co-simulation of mechanics and electromagnetics for dynamic analysis of superconducting maglev vehicles moving with large displacements," *Quarterly report of RTRI*, vol.26, no.5, May 2012.

Gang Lv (M'15) received the Ph.D. degree in electric machine and driven from Beijing Jiaotong Univ., Beijing, China, in 2007.

From 2007 to 2009, he was a Postdoctoral Research Fellow with the Technology Center, CRRC Qingdao Sifang Locomotive and Rolling Stock Co.Ltd., Qingdao, China. In 2007, he joined Sch. of E.E., Beijing Jiaotong Univ., where he is currently a Professor. His research interests include analysis and control of linear machines.

Prof. Lv is a Fellow of the Institution of Engineering and Technology. He has served as chair and organizing committee member for many international conferences. He is a managing director of the Electric Drive Technology Sub-Committee - Electric Vehicle Technical Committee- IEEE PES China.

Yaqing Liu received the B.Eng. degree in electrical engineering from Qilu Univ. of Technology (Shandong Academy of Sciences), Shandong, China, in 2018.

She is currently working toward the Ph.D. degree in electric machine and driven in Beijing Jiaotong Univ., China, where she has been engaged in the linear synchronous machines and maglev.

Zhixuan Zhang received the B.Eng. degree in electrical engineering from Shanxi Univ., Shanxi, China, in 2012.

He is currently working toward the Ph.D. degree in electric machine and driven in Beijing Jiaotong Univ., China, where he has been engaged in the design and analysis of linear synchronous machines.

Xiaodong Li (Senior Member, IEEE) received the B.Eng. degree in electrical engineering from Shanghai Jiao Tong University, Shanghai, China, in 1994, and the M.A.Sc. and Ph.D. degrees in electrical engineering from the University of Victoria, Victoria, BC, Canada, in 2004 and 2009, respectively.

From 1994 to 2002, he was an Electrical Engineer with HongWan Diesel Power Corporation, Zhuhai, China, where he conducted maintenance of the diesel power generation system. In 2009, he joined the Faculty of Information Technology, Macau University of Science and Technology, Macau, China, where he is currently an Associate Professor. He has authored or coauthored more than 50 papers in international conference proceedings and journals and holds four U.S. patents and five Australia Innovation patents. His research interests include high-frequency power converters and its applications.

Dr. Li received the IEEE Power and Energy Society Best Paper Prize in 2007 and the Bank of China Research Excellence Award from the Macau University of Science and Technology in 2013.